Measurement 115 (2018) 1–10

Contents lists available at ScienceDirect

Measurement

journal homepage: www.elsevier.com/locate/measurement

In-situ monitoring and characterization of airborne solid particles in the hostile environment of a steel industry using stand-off LIBS

D. Girón[a], T. Delgado[a,*], J. Ruiz[b], L.M. Cabalín[a], J.J. Laserna[a]

[a] Departamento de Química Analítica, Universidad de Málaga, Facultad de Ciencias, Campus de Teatinos s/n, 29071 Málaga, Spain
[b] Departamento de Física Aplicada I, Universidad de Málaga, Facultad de Ciencias, Campus de Teatinos s/n, 29071 Málaga, Spain

ARTICLE INFO

Keywords:
Laser-induced breakdown spectroscopy
Stand-off analysis
Solid aerosol detection
Steelshop atmosphere
Continuous casting line
Sampling rate

ABSTRACT

The analytical possibilities of laser induced breakdown spectroscopy (LIBS) to carry out in-situ and real-time detection and compositional characterization of aerosols in the atmosphere of a steelmaking factory, have been evaluated. To this aim, a compact and versatile dual-pulse LIBS analyzer, able to sample at distances up to eight meters, has been designed to work in these hostile industrial environments. Due to the discrete nature of the particulate matter, the particle sampling rate was less than 2.5% and 6% for single- and double-pulse regimes, respectively. An efficient statistical procedure, based on the calculation of standard deviations, is used to qualitatively characterize the elemental composition of the aerosol. Then, a conditional analysis based on the limit of detection, is employed to assess the elemental sampling rate. This experimental methodology has been used to evaluate the influence on the aerosol formed of the oxycutting process in a continuous casting machine producing steel slabs, revealing a strong presence of elements derived from the casting powder used in the production. Moreover, chromium, present in the steel cast, is detected in aerosol suspension in the steel shop. An increase in the concentration of particulate matter was expected when oxycutting was on. Single-pulse and dual-pulse excitation modes are also evaluated.

1. Introduction

Air pollution is an old and widespread problem, as well as a modern-day issue. Originating from both natural and anthropogenic sources, contaminants are directly introduced in the atmosphere as gases and particulate matter. In addition, these particles can also come from photochemical processes induced by solar radiation. These airborne particles or atmospheric aerosols are ubiquitous in the environment, and some of them may be hazardous for the environment and health, and affect the economy. Especially adverse effects on human health are due to heavy metal particles that may accumulate in human beings via inhalation and respiratory deposition [1]. So, the analysis of aerosols in ambient air has been a concern of the scientific community in recent years because of those potential adverse effects on health and visibility, and because they play a role in the regulation of climate processes [2–5]. In this context, the acquisition of analytical information of particulate matter present in a specific atmosphere is of a crucial interest.

One of the most important anthropogenic sources of emissions in today's societies is the steelmaking industry. Main processes may include the use of coke as fuel and as a reducing agent in smelting iron ore in a blast furnace [6]. Coke ovens are the major source of polyaromatic hydrocarbon (PAH) emissions in the iron and steel facilities [7]. Furthermore, throughout the steelmaking process, the cutting of the steel bars produced, namely slabs, blooms and billets, is performed after casting in an oxy-fuel unit. In this stage, a torch is used to heat metal to its kindling temperature. Then, a stream of oxygen is guided to the metal, burning it into a metal oxide that flows out of the kerf as slag. Both the combustion of fuel and the produced metal are involved, through a highly energetic reaction, with the inherent generation of particles and combustion gases. Most studies carried out in these industrial environments have focused on the assessment of physical and chemical characteristics of particulate aerosols from important dust sources identified in integrated iron and steel processes, more specifically on sintering, blast furnace, steelmaking and desulfurization slag processing. Fe, Ca, Al, Na, S and Mg have been the major elements usually found [8]. Moreover, the composition of the suspended particulate matter measured around a steel plant has been compared with that of the urban environment [1].

Such chemical diagnoses and the specific analytical techniques used to this aim are becoming more and more relevant. The current methodology consists of the use of particle filtration samplers, combining

* Corresponding author.
E-mail address: tomas.delgado@uma.es (T. Delgado).

http://dx.doi.org/10.1016/j.measurement.2017.09.046
Received 30 June 2017; Received in revised form 1 September 2017; Accepted 26 September 2017
Available online 03 October 2017

different size-selective inlets, filter media, and flow movers/controllers. However, this approach is time-consuming and uses large sampling air volumes [9,10]. Also, as in many common techniques, treatment processes are required for analysis [11].

Surveillance of solid aerosols demands the rapid, remote and *in situ* evaluation of chemical composition and concentration of particulate matter in air. Relevant analytical challenges emerge because of the significant heterogeneity exhibited by aerosol properties (i.e., particle density, size, morphology and composition) [12]. Therefore the use of a compact, robust, and versatile analytical system, as well as the capability of working *in situ* and in real time, would be highly desirable. For years, LIBS has been used to obtain information that allows a better understanding of the dynamics of these polluting agents in the form of solid aerosols. In this context, several research works involving LIBS detection of solid aerosols in ambient air as well as in waste stream effluents for real time monitoring have been reported [13–17]. Thus, LIBS application for aerosols analysis offers many advantages that overcome some of the inherent limitations that the current technologies used for this purpose present. In recent years, this technique has been developed as a novel system for the direct quantitative measurement of particle size [18], extent of oxidation or coating thickness of nanoparticles [19], and separate particulate composition [20]. However, many fundamental issues related to the laser induced plasma interactions with the aerosol particles are still outstanding [12].

The stand-off LIBS approach allows the analysis of physically inaccessible targets or samples which may be located in hazardous environments. Generally, stand-off LIBS systems use nano- or femtosecond pulse lasers for the analysis of both solid and liquid samples located at several meters from the instrument. This approach has been used in numerous and different applications (environmental monitoring, nuclear and metallurgical industries, planetary exploration, cultural heritage, detection and identification of explosives, etc.) [21–24]. Moreover, the possibility to monitor at a safe distance for those cases in which the samples present a risk for both operators and equipment is a clear advantage of this technology [25].

This study aims to demonstrate the stand-off LIBS capability for in-situ analysis of variable-sized heterogeneous solid aerosols in Brownian motion, generated in a real industrial scenario. To the knowledge of the authors, it is the first time that a LIBS system is deployed in a steel factory to detect particulate matter suspended in air. The work focuses on the detection of aerosol particles as well as the determination of their major elemental composition. In order to gather preliminary information, measurements were performed by remote and direct sampling of the environment inside the steel making factory, where diverse metallic elements were expected to be detected. Furthermore, in order to assess the efficiency of the methodology, the intensity variability and the sampling rates were estimated.

2. Experimental

2.1. Stand-off LIBS system

A versatile and compact LIBS portable system was built for industrial tests capable of working in stand-off mode with non-invasive technology. The prototype is shown in Fig. S1 (see Supplementary Material) and has been previously described [26,27].

Two 1064-nm Q-switched Nd:YAG lasers with 5 ns pulse width, and combined in an axial configuration, were used. The combined maximum energy available was 900 mJ at a maximum repetition rate of 10 Hz. The two laser beams were properly synchronized by means of their own internal electronic device, which triggered them with a controlled delay of 2 μs, and then guided, expanded by means of a Galilean telescope, and focused in order to obtain the level of irradiance required to produce aerosol optical breakdown at typical distances of 5 m. Selected optical elements allowed an adequate guiding and focusing of the laser beam and an optimal signal collection.

Collection of the plasma light was carried out by a commercial Maksutov-Cassegrain telescope (f 1/15) and focused with a plano-convex quartz lens (FL 50 mm) onto the input aperture of an optical fiber (D 400 μm). This fiber is connected to the entrance slit of a dual-channel asymmetrical crossed Czerny-Turner spectrometer that detects the dispersed radiation with an integrated linear CCD array of 2048 pixels. The CCD aperture is triggered just 1 μs after the firing of the second laser pulse, and the integration time was fixed at 1.1 ms (the minimum integration width allowed). The grating installed inside each spectrometer has 1200 grooves per mm, and the slit width was 10 μm, providing a spectral resolution of 0.1 nm (FWHM) in the selected spectral region. The spectral range for the combination of both spectrometers covered from 343 to 597 nm, and from 594 to 812 nm respectively, which allowed the detection of the spectral lines of the elements of interest. Measurements were taken alternatively (i.e., at a separate time) for the two spectral ranges since the use of a bifurcated fiber led to the acquisition with a worse signal to noise ratio. The system was protected within an enclosed box away from the hot and dusty environment in the factory. A detailed description of the system can be found elsewhere [26].

The LIBS analyzer and the auxiliary equipment were deployed next to the slab continuous casting line, in the proximity of the oxycutting unit. Fig. 1 shows a scheme of the location of the LIBS analyzer. The final distance from the LIBS system to the slabs in the continuous casting line was 7.6 m, and the laser output was tilted and pointed just in front of the area where oxycutting process of slab took place. The

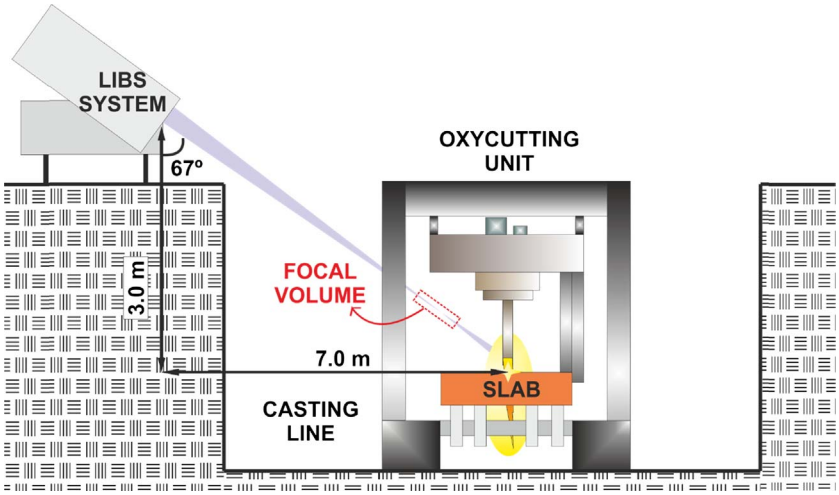

Fig. 1. Schematics of final location for stand-off LIBS analyzer in the steelmaking factory, near the oxycutting area.

laser beams were focused onto a region at around 5.6 m from the LIBS system, approximately at a distance of 2 m from the top surface of the slab. This ensured that the depth of focus (DOF) was separated from the slab surface at all times so that only the aerosol above the surface, and not the surface itself, were analyzed. The beam guiding components play a crucial role since they have to focus the laser energy in a sufficiently small spot in order to provide the necessary irradiance to produce the emission plasma of airborne particles. The minimum achievable spot diameter in such analysis conditions was estimated to be 0.5 mm, taking into account the beam quality parameter (M^2 = 2.95) and the laser beam diameter at focusing optics (D = 40 mm). According to these experimental conditions, the DOF of the laser beam was estimated to be 125 mm.

LIBS measurements have been conducted using two laser excitation approaches, namely single- and double-pulse. In both cases, two situations were compared: experiments carried out while the oxycutting system is running or not. When the double-pulse regime was employed, laser energies of 250 mJ/350 mJ for first and second pulses, respectively, were chosen with a repetition rate set to 5 Hz, whereas for single-pulse, the laser energy was set to 250 mJ. In both cases, the energies involved are enough to generate the breakdown of the sampled aerosol. A value not lower than 2.5×10^{10} W/cm^2 is obtained for these experimental settings when using single-laser pulse mode.

In the search of differences between the two laser excitation modes, particle sampling rates (PSR), defined as the percentage of laser shots that sample at least one particle within the plasma volume [12], were determined. For this estimation, a conditional analysis was performed based on the IUPAC criterion 3 s (threshold value for the limit of detection), which usually corresponds to a confidence level of about 90% [28,29].

LIBS experiments were performed during continuous casting of a ferritic steel grade (AISI 430), whose elemental composition is showed in Table 1.

2.2. Standard deviation and conditional analysis methodologies

Because of the discrete, particulate nature of aerosols, the utilization of LIBS is considered in part as a statistical sampling problem involving the finite laser-induced plasma volume, as well as the concentration and size distribution of the target metal species [30]. The most of the spectra registered consists of background (no spectral peaks). The rest of them are spectra with identified elemental features: we will call breakdown events to this kind of spectra. Some of them contain only spectral lines corresponding to air constituents, while some of them contain spectral features revealing the presence of aerosol (we will call particle hits to this last kind of breakdown events).

Single particle hits generate strongly variable spectral signals for specific species. Despite the high intensity found for some elemental spectral features, a large percentage of laser shots generate spectra free of particle signatures (i.e., only background or lines related to the air constituents), and as a result, the ensemble-averaged intensities are severely reduced.

On the contrary, standard deviation (SD) values for the measured emission intensities become extremely high. Thus, this statistical parameter (SD metric) can be used instead of the absolute LIBS emission intensities to characterize the spectral response of the aerosol particles in low concentration, and, consequently, with a negligible loss of significant information from the analyte. For each ensemble of spectra, a SD spectrum was obtained calculating the standard deviation of the intensities at each wavelength [31]. The SD spectrum thus obtained reveals quickly the spectral lines due to the detected aerosol (and/or air constituents).

A clear evidence of this fact is reflected in Fig. S2, where a comparison of the ensemble-averaged emission intensities and SD metric is presented. As observed, both amplitude and signal-to-noise ratio (SNR) corresponding to SD metric proved to be noticeably higher than the averaged emission intensities. All detected spectral lines appearing in the ensemble-averaged spectra (Fig. S2a) are also present in the SD plot (Fig. S2b), thus confirming that SD method is appropriate for data examination of non-homogeneously dispersed particles. Nevertheless, some assigned elemental lines clearly visible in the SD plot are not present at all in the ensemble-averaged spectra, which proves the interest of this kind of plot [31]. Although the absolute spectral intensity values are lost, the use of the standard deviation method becomes a very powerful tool for further processing of spectral signals with high variability.

The classification of single-shot spectra into two groups, one of them with significant spectral response (breakdown events), and the other without it (only background), can be used to assess the collected data. This evaluation allows achieving more accurate values for the sampling yield, related to particles concentration levels and aerosol composition. This conditional analysis, which increases the signal-to-noise ratio of the spectral data, has been previously described in the study of non-homogenous analyte systems [32]. In this study, the SD spectra were used to determine the spectral lines to be considered in the conditional analysis.

Once the spectral lines to work with have been determined with the SD metric, a criterion has to be adopted to characterize a particle hit. In order to accomplish it, the selection of an appropriate threshold for the intensity of these spectral lines is the essential task to qualify a given spectrum as corresponding to a particle hit or not. When the value of the emission intensity exceeds this threshold, the corresponding single-shot spectrum is classified as representative of a particle hit [33]. The criterion adopted here was that signal-to-noise ratio (SNR) value resulted greater than 3 (according to IUPAC recommendations). Additionally, spectra with SNR values greater than 10 were also taken into account for assessing variability differences between signals belonging to the different sampled volume components, namely particle matter and air matrix constituents. For the present analysis, SNR is defined as the ratio of the atomic emission line net intensity to the standard deviation of the adjacent, featureless, continuum (background). After counting spectra with particle hits, sampling rate values were then computed .

Sampling rate values may be computed for detection of specific elemental lines, for specific species, or in an overall way for all detected elements. So, overall sampling rate accounts for detection of all spectral lines, while particle sampling rate accounts for only particle hits (i.e., only lines related to metallic elements). The sampling rate value for only lines related to air constituents (spectra without lines related to metallic elements) may be drawn from the subtraction of the particle sampling rate to the overall.

Table 1
Elemental composition of the cast steel grade AISI 430. Samples were analyzed by X-ray fluorescence (XRF) and optical emission spectroscopy (Spark-OES) in Acerinox Europe S.A. labs from lollypops samples extracted from tundish during the casting process. EN: European Norm. AISI: American Iron and Steel Institute.

		Concentration (%)								
Steel	EN	Si	Mn	Ni	Cu	Cr	Mo	Nb	Co	V
AISI 430	1.4016	0.42	0.32	0.23	0.05	16.65	0.03	0.01	0.02	0.11

3. Results and discussion

3.1. Spectral analysis of aerosols

The examination of the attained spectra from individual breakdown events permits identification of the relevant elements present in the aerosol particles or air susceptible to rupture; the corresponding spectral lines are summarized in Table 2. In general, most of the breakdown events corresponded to air rupture (where main emission lines

Table 2
Selected spectral lines used for the calculation of the sampling rates, for both spectral ranges.

Range 343–597 nm			Range 594–812 nm		
Element	Ion. Stage	Line (nm)	Element	Ion. Stage	Line (nm)
Ca	II	393.37	Ca	I	616.21
Ca	II	396.85	Ca	I	643.90
Ca	I	422.67	H	I	656.28
Al	I	396.15	Li	I	670.78
Ti	I	453.32	N	I	746.83
Cr	I	520.84	K	I	766.49
Na (doublet)	I	588.99/ 589.59	O (triplet)	I	777.19/ 777.42/777.54

corresponding to H, N and O species are found, but not emission from rest of elements detected), thus confirming that the experimental irradiance level of the LIBS system far exceeds the threshold for air breakdown – air rupture when no aerosols are present - (around 10^{11} W/cm^2). Also, the presence of aerosol particles in the focal volume will lower the threshold for gas breakdown by several orders of magnitude (typically to around 10^7 W cm^{-2}) [34]. On the other hand, a spectral analysis determines that most of the sampled particles are based on both alkali (Li, Na, K) and alkali earth (Ca) compounds. Fig. 2 shows a pair of typical spectra obtained for each of the active channels of the spectrometer (while the oxycutting unit is on) and using double-laser pulse excitation. As observed, the spectrum in Fig. 2a is characterized by the presence of Ca II (393.37 and 396.85 nm) peaks, and the well-known doublet Na I (589.00 and 589.59 nm). On the other hand, the strong emission features corresponding to air rupture are depicted in Fig. 2b, in which O I (triplet not resolved at 777.19, 777.42 and 777.54 nm) LIBS signal governs the spectrum.

Fig. 3 presents three examples of individual laser events exhibiting emission signal of additional metallic species. The LIBS spectra correspond to Ti-, Al- and Cr-containing particles, respectively. Fig. 3a illustrates a representative spectrum for the ablation of a Ti-containing particle, in which lines at 453.48 nm and 499.95 nm become the most intense signals for this element. Fig. 3b shows a detail of a LIBS spectrum where the Al resonant lines at 394.40 nm and at 396.15 nm can be observed. Fig. 3c exhibits a single-shot spectrum with the presence of several Cr emission lines. It should be noted that these elements were detected in a lower number of laser events, compared to Ca, Na and air constituents. This fact will be extensively discussed below (in the section on sampling rates). On the other hand, surprisingly, in spite of being measured inside a steel shop, Fe lines were not identified in any of the laser event measurements.

In addition, CaF and CaO molecular bands have also been detected in some of the emission plasma events, as shown in Fig. 4 [35]. Moreover, in this spectral range, the presence of lithium is revealed by its signature emission line at 670.79 nm.

3.2. Sources of the particulate matter. Steel slab and casting powder

In the steel manufacturing process, once the steel is cast, the resulting slabs/billets have to be cut. The process of cutting with an oxygen flux -or oxycutting- is the most common in steel industry. This aggressive process is performed with an iron powder supply and an oxygen stream, releasing large amounts of energy on a previously heated metal (near the ignition point of the material). Furthermore, in order to facilitate the cutting of the stainless steel slab, iron powder is provided using compressed air or nitrogen. As the powder burns, a great deal of heat is generated resulting in the formation of a viscous slag due to the combination of combustion phenomena with the melt action of the flame. This slag consists mainly of chromium oxides that opposes

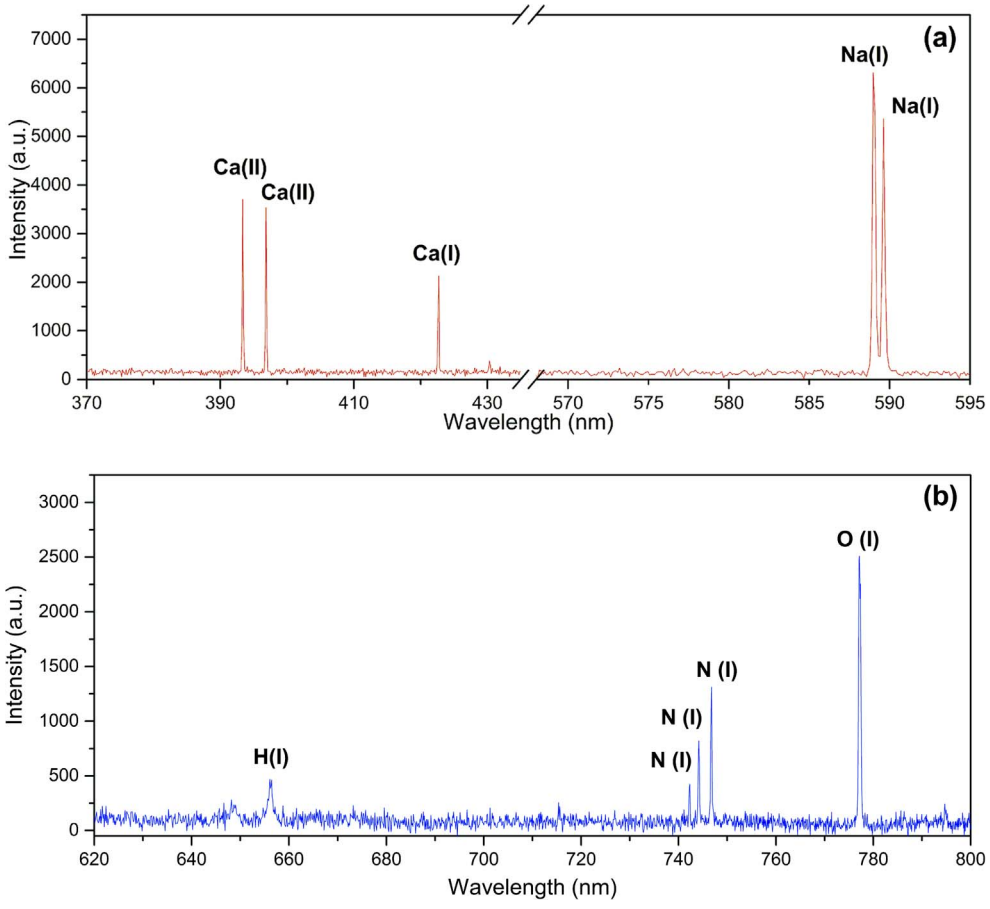

Fig. 2. Typical spectra acquired from single-shot for (a) Ca/Na based particle aerosol, first channel (b) air rupture, second channel. Double-pulse scheme was performed when the oxycutting system was on.

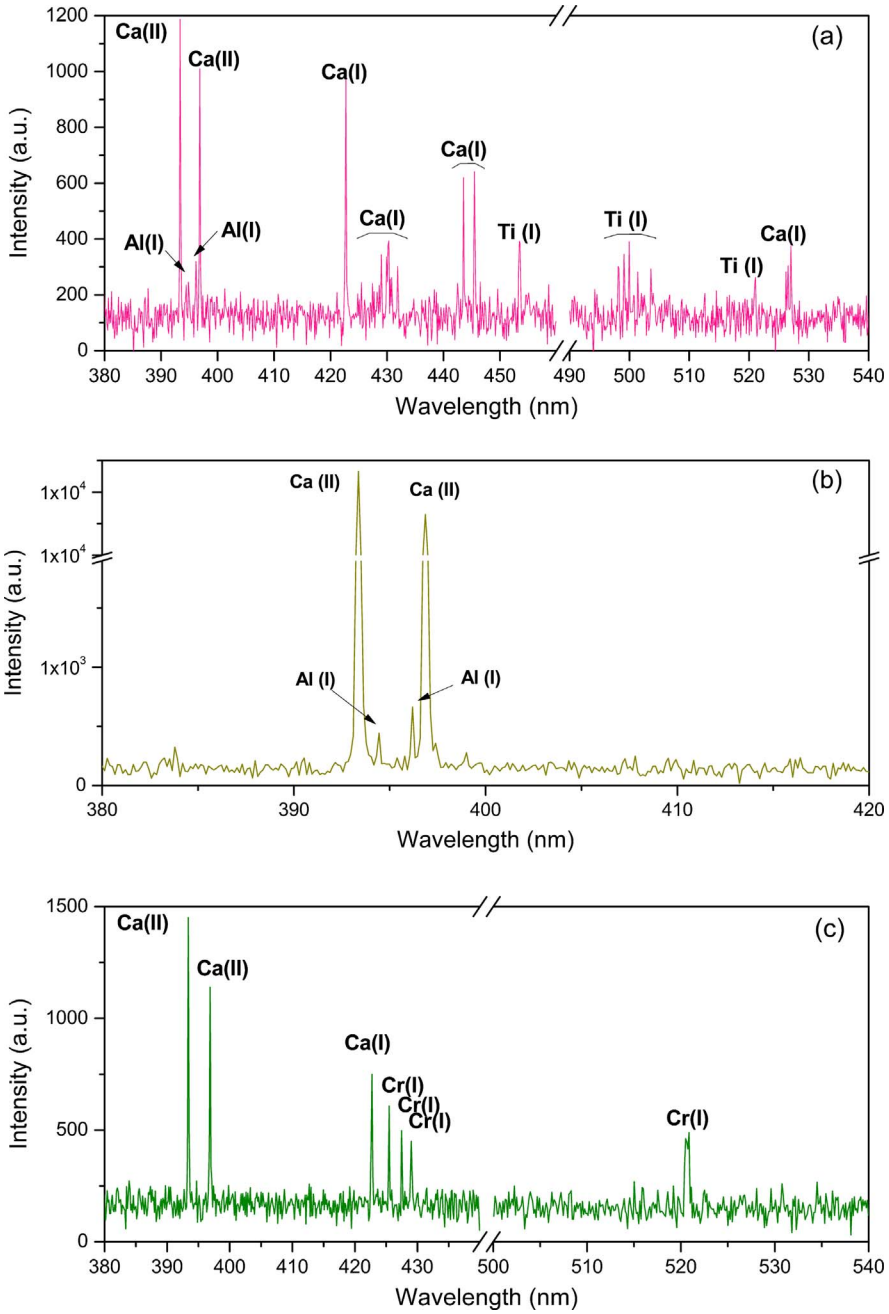

Fig. 3. Three examples of single-shot LIBS spectra for (a) Ti-containing particle, (b) Al-containing particle (only a detail of spectral range is presented), (c) Cr-containing particle. Double-pulse scheme was performed when the oxycutting system was on.

the action of the oxygen flame [36]. In order to help the heat dissipation, the oxycutting process is water cooled. It is reasonable to think that this device could be one of the main sources of aerosols generation in this industrial environment. For this reason, field trials were carried out nearby the steel oxycutting unit.

In order to gain evidence on the origin of the different elemental species observed during aerosol monitoring, two different spectra were measured and compared. Fig. 5a shows the real-time LIBS spectrum focusing the laser beam precisely onto the slab surface (at around 900 °C), at a distance of 7 m from the laser, while the steel was being cast at a speed of ca. 1 m/min. The spectrum shown is the average of 100 laser shots at different fresh positions of the slab surface. In this spectrum, the main emission features of ferritic steel are observed: Fe spectral lines, accompanied by some lines of chromium and manganese as major alloy elements. However, strong emission peaks (mainly of Ca-containing species), due to elements not present in the chemical composition of the stainless steel, are also detected [27]. These unexpected spectral emissions have been demonstrated to come from the scale layer formed on the top surface of the steel, contaminated with rests of the casting powder (used to ensure the reliability of the continuous casting process). These casting powders or mould fluxes are synthetic slags constituted by a complex mix of oxides, with fluorite and carbonaceous materials in their composition. The chemical content of the mould flux employed during the experimental measurements is detailed in Table 3. Fig. 5b shows a LIBS spectrum of a mould powder pellet, acquired in the laboratory at a high temperature, simulating the experimental conditions of the casting line, and averaging 20 laser shots on the same spatial position of the sample. A comparison of Fig. 5a and b proves the presence of remains of mould powder spread on the slab surface examined at the steel shop. Species as Ca, Na, Li, Al, Ti and Mg were identified in both spectra. Ti emission, for instance, is well observed despite its low concentration (TiO_2 < 0.7%). CaO molecular bands are also observed; the congested green band around 550 nm, and the much stronger orange-band around 620–630 nm. However, it should be noted

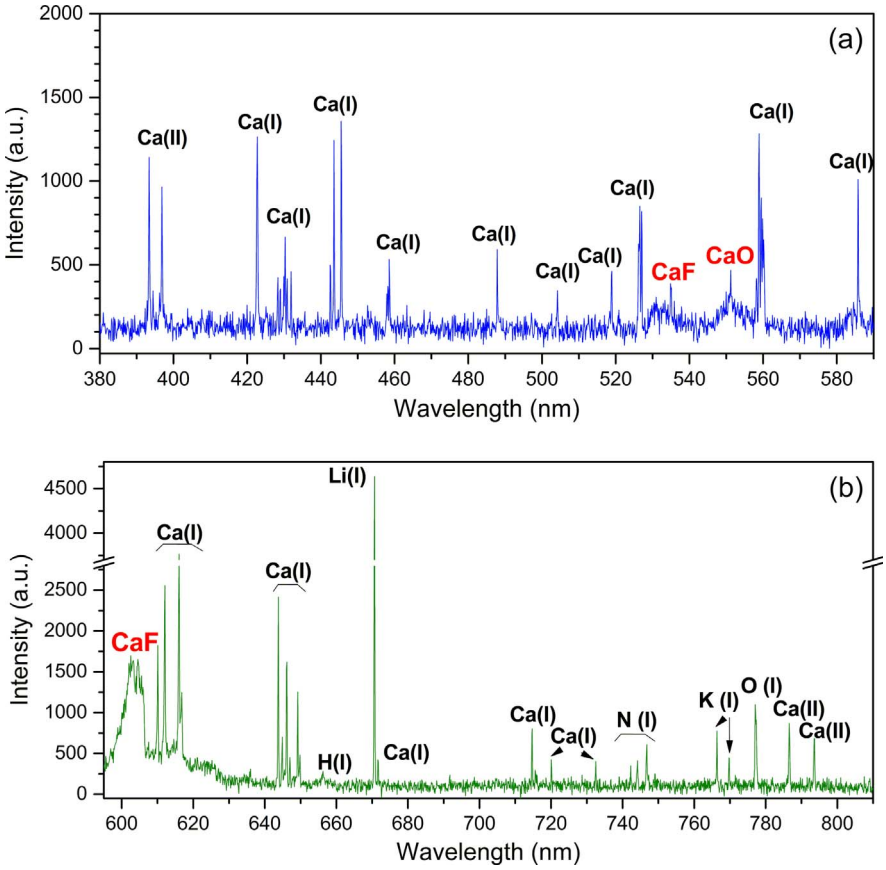

Fig. 4. Two examples of single-shot LIBS spectra for ablation of particulate material likely containing mould powder particles: (a) without Li emission, (b) with Li emission. Double-pulse scheme was performed when the oxycutting system was on.

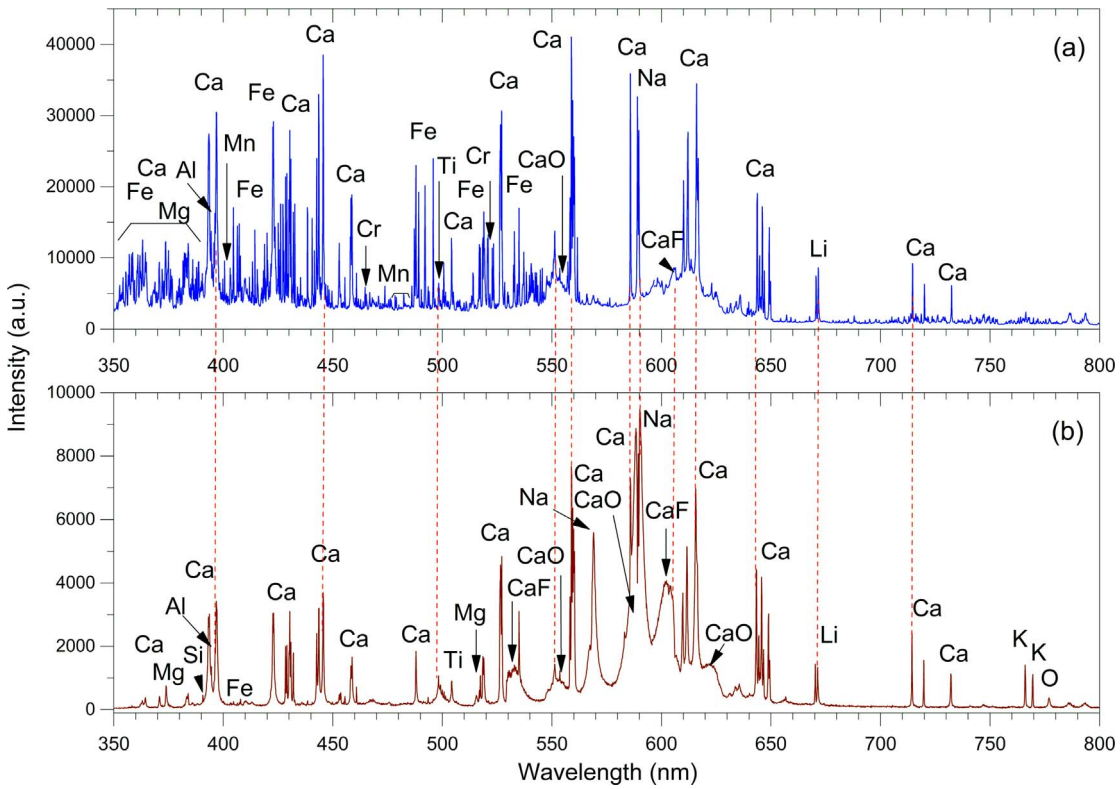

Fig. 5. Real-time LIBS spectra corresponding to (a) stainless steel AISI 430 acquired at high temperature during continuous casting; (b) pellet of mould powder acquired in the laboratory at 900 °C in similar experimental conditions. Laser operating in double-pulse mode and focusing the laser beam on the sample surface. Two spectrometer channels were connected simultaneously for light collection using a bifurcated-400 μm diameter fiber.

Table 3
Elemental composition of mould powder used in the casting process. Supplied concentrations are averaged values. Synthetic slag density was about 0.64 g/cm^3 and the grain-size was lower than 1.0 mm. Composition was provided by the commercial technical data sheet.

Concentration (%)												
Mould powder	SiO_2	CaO	Na_2O	CO_2	Al_2O_3	CaF_2	MgO	C_{free}	TiO_2	Fe_2O_3	K_2O	MnO_2	Li_2O
MP-1	35.2	30.9	11.2	8.8	5.8	4.0	2.3	1.3	< 0.7	< 1.0	< 0.5	< 0.5	< 0.5

that, although iron is also present in the chemical composition of the mould powder in low concentrations, in the form Fe_2O_3 (< 1%), and it is not easily detectable, Fe lines (at 404.58, 406.36 and 407.17 nm) could be identified as indicated in Fig. 5b.

Elements as Ca, Na and K are present in many of the particle hits (see Figs. 2, 3 and 4), since they take part of the main oxides existing in the mould powder composition. Moreover, these atomic species are easily ionizable and their ablation and excitation thresholds are low.

The detection of Li in some of the collected spectra from aerosols could be attributed to its presence - in very low levels (< 0.5%) - in the mould powder composition, as it is also observed in the LIBS spectrum of the mould powder pellet. However, its presence in the aerosol could also be associated to lithium soap. This kind of grease, used for the lubrication of rollers and bearings of continuous casting lines, as well as the hot-rolling mill, is a Li-based compound. This lithium soap could eventually be evaporated, leaving behind an inorganic remnant enriched in lithium, due to the high temperatures of the slab and generated in the oxycutting process. Notwithstanding, there is no evidence of organic molecular bands (CN, C_2, CH, NH, OH…) in the collected spectra that could confirm such an origin; this source may not be excluded as secondary source since the emission intensity of Li achieved is often very significant in the aerosol, as observed in spectrum depicted in Fig. 5b. The observation of CaO and CaF molecular bands, characteristic of the particulate matter spectra, is an additional fact supporting that casting powder is the main source of the measured aerosols.

Furthermore, the only metallic species detected in the aerosol analysis, but not present in the casting powder, is chromium, the main alloying element of the steel grade cast, as observed in Fig. 3c. In this case, its origin can be associated unequivocally to the scale layer formed on the surface of the slab. This layer is enriched in chromium oxides due to the diffusion of Cr atoms from the bulk to the external regions of the slab, favored by high temperatures in the casting process [37,38]. The lower density of the scale layer compared to that of the steel (7.8 g/cm^3), along with the weak joining to the slab surface, allows the pulverization of the oxidized layer in the oxycutting process, thus generating Cr-containing particles in the aerosol. Volatility of chromium oxides has been widely studied [39,40] as well as the oxidation of steel in different atmospheres and temperature ranges [37,41,42].

3.3. Signal variability

Once the suspended material has been spectrally identified in the steel shop atmosphere, and its most probable origins discussed, the next step to be carried out is a statistical study of the data. Due to the nature of the particulate matter, a large signal variability is expected.

The uncertainty of measurements is assessed by means of the ensemble-average of the intensities and SNR values. These values were calculated after applying a conditional analysis to the spectra, as discussed in the Experimental Section, and are summarized in Table 4. The relative standard deviation (RSD) of the ensemble-average values of net intensities and SNR, for the sets of spectra with SNR greater than 3 and greater than 10, respectively, were computed. These results, for spectral lines corresponding to both particulate matter and air matrix constituents, were then compared. The most intense spectral lines used for this purpose were: for particulate matter, Ca II at 393.37 and 396.85 nm, measured from particle hits breakdown events. For air matrix constituents, N I at 744.23 and 746.83 nm, and the O I triplet, not spectrally resolved, at 777.19, 777.42 and 777.54 nm, measured from just only-air breakdown events. This statistical study has been performed using single- and double-laser pulse regimes.

Table 4
Relative standard deviation (RSD) values calculated from the averages of both spectral intensities (Int.) and signal-to-noise-ratio (SNR) values for the set of spectra whose SNR is greater than 3 and 10 respectively, for the examined elemental spectral lines, in experiments carried out using double- and single-pulse excitation.

Ensemble	Line (nm)	Double-pulse		Single-pulse	
		Int. RSD (%)	SNR RSD (%)	Int. RSD (%)	SNR RSD (%)
SNR > 3	Ca II 339.37	39	172	28	100
	Ca II 396.86	37	180	26	109
	N I 744.23	15	46	15	47
	N I 746.83	22	62	23	61
	O I 777[a]	33	70	27	62
SNR > 10	Ca II 339.37	43	132	32	72
	Ca II 396.86	41	139	29	73
	N I 744.23	11	15	7	22
	N I 746.83	20	27	10	47
	O I 777[a]	25	40	25	34

[a] Triplet not spectrally resolved.

As can be observed in Table 4, uncertainties computed for SNR values (in terms of the RSD of ensemble-averaged values) are systematically larger than those calculated for the spectral intensities, since the variability of the background is lower than that of the signals. When the RSD values of all spectral data with SNR > 3 are compared with only those with SNR > 10, differences are found between the constituent elements of particles (calcium) and air (nitrogen and oxygen).

In the case of calcium, the RSD values calculated for spectral intensities in the ensemble SNR > 3 are lower than the values for the subset corresponding to SNR > 10. This fact could be attributed to a number of variables, including the presence of a larger number of sampled lower-size particles, the calcium content level for each particle, and the higher variability of the sampled major-size particles (the number of large particles is lower).

In contrast, in the case of elements present in air, as nitrogen or oxygen, RSD values behave in the opposite way. For the SNR > 3 spectra ensemble, RSD values are higher than the values obtained from the subset with SNR > 10. These results confirm the heterogeneity of the particles sampled. Indeed, as listed in Table 4, the intensity RSD for air constituents (N, O) is significantly lower than that corresponding to particle hits. This result suggests that the excess uncertainty is due to the variable mass of the particles involved. However, as the number of LIBS measurements is not similar in all the cases, due to the random nature of the experiment, this kind of conclusions is not straightforward. Moreover, the discrete behavior of an particle hit, in terms of particle size, composition, density of particles in the interrogated pathway (focal volume where plasma threshold is attained) and so on, is a major source of uncertainty.

Table 5
Summary of overall sampling rate values for tested conditions, expressed in percent (%). For both excitation schemes, values were calculated for data acquired during active and inactive oxycutting process (denoted in the table as Oxyc. on/off, respectively).

Range	Double-pulse		Single-pulse	
	Rate (Oxyc. on)	Rate (Oxyc. off)	Rate (Oxyc. on)	Rate (Oxyc. off)
343–597 nm	6	4	2	3
594–812 nm	23	20	19	23
	1[a]	0.6[a]	0.5[a]	0.8[a]

[a] Spectra excluding events with only-air-rupture features.

3.4. Sampling rates

As it has been defined in the Experimental section, particle sampling rates (PSR) were obtained from the calculation of percentage of laser shots which spectra contain significant lines related to metallic elements, as well as overall sampling rates were obtained but accounting every spectral lines. Again, the studies were carried out (while the oxycutting unit is working) and using single- and double-pulse laser excitation.

Table 5 compares the computed values of the overall sampling rates (i.e., counting the overall significant lines), measured while the oxycutting process is working and while it is off, and under the two different excitation approaches (single and double-pulse). These values have been obtained in two different spectral ranges. In the second spectral range, most of the breakdown events correspond apparently to only air-rupture, obscuring the interpretation in terms of particulate matter detection. The sampling rate for only air breakdown events, which can be inferred from the sampling rate values calculated in the second spectral range, providing values between 19 and 23% of the total of laser shots, regardless the operating conditions (and taking into account that species emission from discrete aerosol particles appearing in this spectral range were always concomitant to air emission). Despite the air is always present, these values are due to the variability related to the plasma formation throughout the depth of focus.

On the other hand, results suggest a moderate impact of the oxycutting process in the average of the sampling rate values, at least in the case of double-pulse excitation, and therefore, a slightly higher concentration of discrete particles in the environment during and immediately after the steel-cutting interval. This small impact of the oxycutting process is inside the expected experimental error for sampling rate values, and the trend is the opposite in the case of single pulse operation of the laser. It should be noted that the results acquired in both excitation modes, namely single-pulse and dual-pulse, are not comparable between them; as the energy delivered in double pulse mode is higher, the particle sampling rate increases [21].

Finally, specific sampling rates corresponding to each detected element were computed and compared in Fig. 6. For example, Cr detection exhibits a maximum value of 0.2%. Taking into account that particle sampling rates calculated by LIBS are on the order of 0.1% for many aerosol loading conditions [30,43], this value may be considered as significant and corresponding to a notable concentration. It has been demonstrated that for submicrometer sized metal particle distributions, and for effluent levels of about 10 μg/acm (typical of many treatment process wastestreams), LIBS particle sampling rates may be in the order of 1% or less, compatible with the values obtained in our experiments [30].

Several conclusions can be drawn from Fig. 6. First, the number of LIBS spectra where Ca lines are detected (Ca sampling rate) was calculated in order to know its statistical weight with respect to the total of the breakdown events (in both spectral ranges). In the first spectral range, Ca sampling rate while the oxycutting was active represents the 87% of the total of the breakdown events. On the other hand, this value is reduced to 3% in the second spectral range, under the same experimental conditions, as a result of the presence of air rupture. If spectra with only air emission signals are not taken into account, the number of events including Ca emission represents the 71% for the second spectral channel, value closer to 87% obtained for the first one. Second, the oxycutting process seems to increase the probability of the ablation mechanism, and the further excitation and emission of Ca and metallic elements (Cr, Ti, Al). However, particle hits corresponding to emission of alkali metals (Li, Na and K) were detected in the environment independently of the laser excitation mode as well as the presence of the oxycutting process.

4. Conclusions

In this study, the analytical possibilities of in-situ detection of solid aerosols generated in a steelmaking factory, as well as the determination of their elemental composition, have been evaluated, using a stand-off LIBS analyzer able to work at distances up to 8 m. Two modes of interaction between laser beam and airborne particles, namely single-pulse and double-pulse laser regimes, were assessed. Experimental results confirmed the main source forming aerosol particles: casting powder probably removed from the slab surface during the oxycutting process of stainless steel slabs. Both elemental (Ca, Al, Ti, Li) and molecular (CaO, CaF) emission signals confirmed the presence of particles

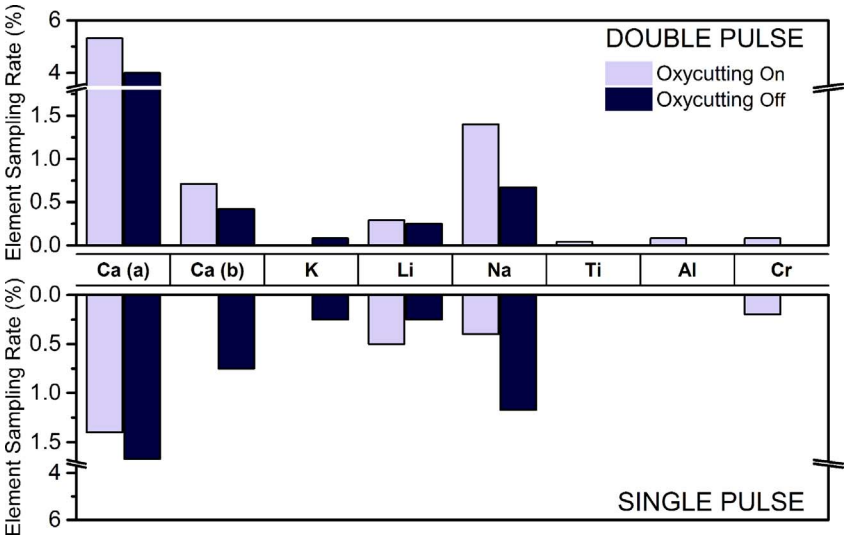

Fig. 6. Sampling rate values for individual species, expressed in (%), measured when the oxycutting unit was on (light bar) and off (dark bar). Ca (a) detected in the spectral range 343–597 nm. Ca (b) detected in the spectral range 594–812 nm.

of the casting powder in the analyzed atmosphere. An additional identified source of particulate matter, obviously, was the steel itself being cut, since Cr emission, coming either from the steel bulk or from the oxidized steel surface, was also detected in the aerosol suspension. Computed values for sampling rates from the analysis of aerosols in a region next to the oxycutting unit are compatible with an enhancement of the concentration of airborne particles during the oxycutting process of the slabs, compared to periods with the oxycutting unit off, although the small differences are inside the expected value for experimental errors. Likewise, double-pulse laser measurements seem to slightly improve the sampling rate values compared to those obtained in single-pulse regime.

Field tests have proved the viability of stand-off LIBS technology for the in-situ and real-time detection of solid aerosols in industrial environments, thus becoming an analytical on-line tool for a rapid monitoring and control of particulate emissions generated in hostile scenarios.

Acknowledgements

This work was financially supported by Dirección General de Investigación Científica y Técnica (DGICT), Spanish Ministerio de Educación y Ciencia, under the contract CTQ2014-56058-P.

The authors kindly acknowledge to D. Pérez and colleagues, of ACERINOX EUROPA S.A.U., for their hospitality and assistance during the field campaign carried out in Los Barrios, Cádiz (Spain) in February 2016, as well as for the experimental characterization of the stainless steel slabs described along this manuscript.

The authors would like to thank the valuable comments and suggestions of reviewers, which have improved the manuscript.

Appendix A. Supplementary material

Supplementary data associated with this article can be found, in the online version, at http://dx.doi.org/10.1016/j.measurement.2017.09.046.

References

[1] Q.L. Dai, X.H. Bi, J.H. Wu, Y.F. Zhang, J. Wang, H. Xu, et al., Characterization and source identification of heavy metals in ambient PM10 and PM2.5 in an integrated Iron and Steel industry zone compared with a background site, Aerosol. Air Qual. Res. 15 (2015) 875–887, http://dx.doi.org/10.4209/aaqr.2014.09.0226.

[2] U.S. Environmental Protection Agency, Revised Standards for Hazardous Waste Combustors. Waste Inciner. Public Heal., 1996, p. 17358–536.

[3] N.R. Council, Research Priorities for Airborne Particulate Matter. Part II. Evaluating Research Progress and Updating the Portfolio. Washington, DC, 1999.

[4] A. Dinoi, A. Donateo, F. Belosi, M. Conte, D. Contini, Comparison of atmospheric particle concentration measurements using different optical detectors: potentiality and limits for air quality applications, Measurement 106 (2017) 274–282, http://dx.doi.org/10.1016/j.measurement.2016.02.019.

[5] J.H. Seinfeld, S.N. Pandis, Atmospheric Chemistry and Physics: From Air Pollution to Climate Change, John Wiley & Sons Inc, New York, 2006.

[6] Chisholm H. Coke, Encycl Br, 657, 1911.

[7] J.H. Tsai, K.H. Lin, C.Y. Chen, J.Y. Ding, C.G. Choa, H.L. Chiang, Chemical constituents in particulate emissions from an integrated iron and steel facility, J. Hazard Mater. 147 (2007) 111–119, http://dx.doi.org/10.1016/j.jhazmat.2006.12.054.

[8] D. Hleis, I. Fernández-Olmo, F. Ledoux, A. Kfoury, L. Courcot, T. Desmonts, et al., Chemical profile identification of fugitive and confined particle emissions from an integrated iron and steelmaking plant, J. Hazard Mater. 250–251 (2013) 246–255, http://dx.doi.org/10.1016/j.jhazmat.2013.01.080.

[9] K.S. Kumar, S. Chellam, C. Lee, M.P. Fraser, Trace elemental analysis of airborne particulate matter using dynamic reaction cell inductively coupled plasma – mass spectrometry: application to monitoring episodic industrial emission events, Anal. Chim. Acta 686 (2011) 40–49, http://dx.doi.org/10.1016/j.aca.2010.11.037.

[10] A. Eiguren-Fernandez, G. Lewis, S. Spielman, S. Hering, Time-resolved chemical characterization of aerosol particles down to 6 nm Diameter in Stockton, California, AIP Conf. Proc. 1527 (2013) 483–486, http://dx.doi.org/10.1063/1.4803310.

[11] M. Radojevic, V.N. Bashkin, Practical Environmental Analysis, second ed., RSC Publishing, 2006.

[12] D.W. Hahn, U. Panne, LIBS for aerosols analysis, in: P. Jagdish, S.N.T. Singh (Eds.), Laser-Induced Break. Spectrosc., Elsevier B.V., 2007.

[13] D.W. Hahn, M.M. Lunden, Detection and analysis of aerosol particles by laser-induced breakdown spectroscopy, Aerosol. Sci. Technol. 33 (2000) 30–48, http://dx.doi.org/10.1080/027868200410831.

[14] G. Gallou, J.B. Sirven, C. Dutouquet, Bihan O Le, E. Frejafon, Aerosols analysis by LIBS for monitoring of air pollution by industrial sources, Aerosol. Sci. Technol. 45 (2011) 918–926, http://dx.doi.org/10.1080/02786826.2011.566899.

[15] M.A. Awan, S.H. Ahmed, M.R. Aslam, I.A. Qazi, M.A. Baig, Determination of heavy metals in ambient air particulate matter using laser-induced breakdown spectroscopy, Arab. J. Sci. Eng. 38 (2013) 1655–1661, http://dx.doi.org/10.1007/s13369-013-0548-7.

[16] U. Panne, Analysis of heavy metal aerosols on filters by laser-induced plasma spectroscopy, Spectrochim. Acta Part B At. Spectrosc. 56 (2001) 839–850, http://dx.doi.org/10.1016/S0584-8547(01)00209-9.

[17] J.E. Carranza, B.T. Fisher, G.D. Yoder, D.W. Hahn, On-line analysis of ambient air aerosols using laser-induced breakdown spectroscopy, Spectrochim. Acta Part B At. Spectrosc. 56 (2001) 851–864, http://dx.doi.org/10.1016/S0584-8547(01)00183-5.

[18] J.E. Carranza, D.W. Hahn, Assessment of the upper particle size limit for quantitative analysis of aerosols using laser-induced breakdown spectroscopy, Anal. Chem. 74 (2002) 5450–5454, http://dx.doi.org/10.1021/ac020261m.

[19] D. Mukherjee, A. Rai, M.R. Zachariah, Quantitative laser-induced breakdown spectroscopy for aerosols via internal calibration: application to the oxidative coating of aluminum nanoparticles, J. Aerosol. Sci. 37 (2006) 677–695, http://dx.doi.org/10.1016/j.jaerosci.2005.05.005.

[20] P. Diwakar, P. Kulkarni, M.E. Birch, New approach for near-real-time measurement of elemental composition of aerosol using laser-induced breakdown spectroscopy, Aerosol. Sci. Technol. 46 (2012) 316–332, http://dx.doi.org/10.1080/02786826.2011.625059.

[21] B. Sallé, P. Mauchien, S. Maurice, Laser-induced breakdown spectroscopy in open-path configuration for the analysis of distant objects, Spectrochim. Acta - Part B At. Spectrosc. 62 (2007) 739–768, http://dx.doi.org/10.1016/j.sab.2007.07.001.

[22] S. Palanco, J.M. Baena, J.J. Laserna, Open-path laser-induced plasma spectrometry for remote analytical measurements on solid surfaces, Spectrochim. Acta - Part B At. Spectrosc. 57 (2002) 591–599, http://dx.doi.org/10.1016/S0584-8547(01)00388-3.

[23] R.S. Harmon, R.E. Russo, R.R. Hark, Applications of laser-induced breakdown spectroscopy for geochemical and environmental analysis: a comprehensive review, Spectrochim. Acta Part B At. Spectrosc. 87 (2013) 11–26, http://dx.doi.org/10.1016/j.sab.2013.05.017.

[24] K. Lee, S. Choi, J.J. Yoh, Stand-off laser-induced breakdown spectroscopy of aluminum and geochemical reference materials at pressure below 1 torr, Spectrochim. Acta Part B At. Spectrosc. 101 (2014) 335–341, http://dx.doi.org/10.1016/j.sab.2014.06.009.

[25] I. Gaona, J. Serrano, J. Moros, J.J. Laserna, Range-adaptive standoff recognition of explosive fingerprints on solid surfaces using a supervised learning method and laser-induced breakdown spectroscopy, Am. Chem. Soc. 86 (2014) 5045–5052, http://dx.doi.org/10.1021/ac500694j.

[26] T. Delgado, J. Ruiz, L.M. Cabalín, J.J. Laserna, Distinction strategies based on discriminant function analysis for particular steel grades at elevated temperature using stand-off LIBS, J. Anal. At. Spectrom. 31 (2016) 2242–2252, http://dx.doi.org/10.1039/C6JA00219F.

[27] J. Ruiz, T. Delgado, L. Cabalín, J. Laserna, At-line monitoring of continuous casting sequences of steel using discriminant function analysis and dual-pulse laser-induced breakdown, J. Anal. At. Spectrom. 32 (2017) 1119–1128, http://dx.doi.org/10.1039/C7JA00093F.

[28] H. Freiser, G.H. Nancollas, Compendium of Analytical Nomenclature (Definitive Rules 1987), Blackwell Science, 1987.

[29] V. Thomsen, D. Schatzlein, D. Mercuro, Limits of detection in spectroscopy, Pure Appl. Chem. 18 (2003) 112–114.

[30] D.W. Hahn, W.L. Flower, K.R. Hencken, Discrete particle detection and metal emissions monitoring using laser-induced breakdown spectroscopy discrete particle detection and metal emissions monitoring using laser-induced breakdown spectroscopy, Appl. Spectrosc. 51 (1997) 1836–1844, http://dx.doi.org/10.1366/0003702971939659.

[31] L.A. Álvarez-Trujillo, A. Ferrero, J.J. Laserna, Preliminary studies on stand-off laser induced breakdown spectroscopy detection of aerosols, J. Anal. At. Spectrom. 23 (2008) 885–888, http://dx.doi.org/10.1039/b716762h.

[32] A. Ferrero, J.J. Laserna, D.W. Hahn, Alternative statistical methods for spectral data processing: applications to laser-induced breakdown spectroscopy of gaseous and aerosol systems, Appl. Spectrosc. 62 (2008) 1144–1152.

[33] J.E. Carranza, K. Iida, D.W. Hahn, Conditional data processing for single-shot spectral analysis by use of laser-induced breakdown spectroscopy, Appl. Opt. 42 (2003) 6022–6028, http://dx.doi.org/10.1364/AO.42.006022.

[34] U. Panne, D.W. Hahn, Analysis of aerosols by LIBS, in: A. Miziolek VP and IS (Ed.), Laser-Induced Break. Spectrosc., Cambridge University Press, New York, 2006, p. 216.

[35] C. Álvarez, J. Pisonero, N. Bordel, Quantification of fluorite mass-content in powdered ores using a Laser-Induced Breakdown Spectroscopy method based on the detection of minor elements and CaF molecular bands, Spectrochim. Acta - Part B At. Spectrosc. 100 (2014) 123–128, http://dx.doi.org/10.1016/j.sab.2014.07.024.

[36] M.F. McGuire, Stainless Steel for Design Engineers, first ed., ASM International, 2008.

[37] G.L. Wulf, M.B. McGirr, G.R. Wallwork, Theoretical analysis of alloy oxidation with reference to Fe-Cr alloys, Corros. Sci. 9 (1969) 739–754, http://dx.doi.org/10.1016/S0010-938X(69)80080-6.

[38] D.J. Young, J. Zurek, L. Singheiser, W.J. Quadakkers, Temperature dependence of oxide scale formation on high-Cr ferritic steels in Ar–H_2–H_2O, Corros. Sci. 53 (2011)

2131–2141, http://dx.doi.org/10.1016/j.corsci.2011.02.031.
[39] B.B. Ebbinghaus, Thermodynamics of gas phase chromium species: the chromium oxides, the chromium oxyhydroxides, and volatility calculations in waste incineration processes, Combust. Flame 93 (1993) 119–137, http://dx.doi.org/10.1016/0010-2180(93)90087-J.
[40] M. Stanislowski, E. Wessel, K. Hilpert, T. Markus, L. Singheiser, Chromium vaporization from high-temperature alloys, J. Electrochem. Soc. 154 (2007) A295, http://dx.doi.org/10.1149/1.2434690.
[41] L.F. Li, Z.H. Jiang, Y. Riquier, High-temperature oxidation of duplex stainless steels in air and mixed gas of air and CH_4, Corros. Sci. 47 (2005) 57–68, http://dx.doi.org/10.1016/j.corsci.2004.05.008.
[42] H. Asteman, J.E. Svensson, L.G. Johansson, Evidence for chromium evaporation influencing the oxidation of 304L: the effect of temperature and flow rate, Oxid. Met. 57 (2002) 193–216, http://dx.doi.org/10.1023/A:1014877600235.
[43] D.W. Hahn, Laser-induced breakdown spectroscopy for sizing and elemental analysis of discrete aerosol particles, Appl. Phys. Lett. 72 (1998) 2960–2962, http://dx.doi.org/10.1063/1.121507.